Transition Polarizability Model of Induced Resonance Raman Optical Activity

Shigeki Yamamoto[a] and Petr Bouř*[b]

Induced resonance Raman optical activity (IRROA) proved to be a very sensitive method to detect molecular chirality. It is exhibited, for example, by complexes of lanthanides with chiral alcohols or ketones. So far, the phenomenon has not been understood at a quantitative level. To elucidate its mechanisms and to correctly relate the spectra to the structure, a transition polarizability model (TPM) is developed and applied to a camphor-europium complex. The model well reproduces the high ROA/Raman intensity ratio of the IRROA observed experimentally. The results additionally indicate a fundamental role of the nonchiral fod ligand in the Eu(fod)$_3$ compound for the chirality enhancement. The TPM model thus serves as a guidance for both experimental and theoretical studies to come.

DOI: 10.1002/jcc.23370

Introduction

Molecular chirality, the left- and right-hand symmetry, is particularly important for biologically relevant systems. For example, proper separation and characterization of enantiomers are essential for medical drugs as they may act differently in a living organism.[1] However, only a limited number of methods can be employed for the detection and monitoring of the absolute configuration (AC). For example, x-ray crystallography requires high quality crystals and the presence of a heavy atom in the molecule.[2] Optical rotation[3–5] or ultraviolet circular dichroism (UVCD)[4,6] can be applied to chiral molecules including solutions or neat liquids, but UVCD is not useful for systems not absorbing in the UV region, such as sugars.[6] Vibrational optical activity spectroscopies including the vibrational circular dichroism and vibrational Raman optical activity (ROA) provide a more reliable AC and conformational resolution than the electronic methods such as UVCD, but require long accumulation times and high sample concentrations.[7]

Lately, the induced resonance ROA (IRROA) emerged as a more sensitive technique for this purpose. It is observed, for example, when a chiral alcohol or ketone makes a complex with (achiral) europium complex Eu(fod)$_3$ in solution.[8,9] The europium ion provides electronic transitions in resonance with the laser excitation wavelength, and consequently large polarizability and intense Raman signal.[7–11] The ROA, that is, the difference in the scattering intensities between the right- and left-circularly polarized light, is induced in the europium electronic cloud by the chiral adduct.

Compared to conventional ROA monitoring vibrational transitions only, IRROA provides a much larger circular intensity difference (CID) ratio of the ROA/Raman signals, which is due to the direct participation of electronic transitions. For the europium complexes, the energy of the $^7F \rightarrow {}^5D$ transitions of the Eu^{III} ion is close to that of the laser excitation wavelength of 532 nm, and the ^7F ground state is split to electronic sublevels with energy gaps ranging from 360 to 5300 cm^{-1}.[8–11] The measurement that can be performed on standard ROA spectrometers is very fast indeed (minutes) and a small amount (micrograms) of the sample is needed. The IRROA spectral patterns are sensitive to the chiral analytes, whereas negligible shift is observable in the Raman band positions. If the link between the fine IRROA pattern and the structure is understood one day, the technique could be used for an extremely efficient detection and recognition of chiral compounds.

So far, the precise relation of IRROA to the structure is not known. Contemporary computational chemistry provides only limited means of accurate treatment of the high-spin lanthanide compounds requiring open-shell and relativistic approaches.[12] Additionally, because of the intertplay between the energetically close electronic and vibrational transitions, an approach beyond the Born–Oppenheimer one may be needed to reproduce all aspects of the experiment.

Fortunately, basic insight can be obtained by a simplified treatment. In this work, we present a semiclassical model where the metal ion (typically Eu^{3+}) is represented by a polarizable sphere, allowing also for a transitional polarizability. This approach can be thought of as an extension of the concepts previously employed in the theoretical studies of surface-enhanced Raman scattering (SERS) and surface-enhanced ROA (SEROA).[13–15] The electromagnetic field of the laser is treated classically, whereas molecular properties are obtained from

[a] S. Yamamoto
Department of Chemistry Graduate School of Science, Osaka University, Toyonaka, Osaka 560-0043, Japan
[b] P. Bouř
Institute of Organic Chemistry and Biochemistry, Academy of Sciences, Flemingovo náměstí 2, 16610 Prague, Czech Republic
E-mail: bour@uochb.cas.cz
Contract grant sponsor: Czech Science Foundation; Contract grant number: P208/11/0105 and 13-03978S; Contract grant sponsor: Academy of Sciences; Contract grant number: M200551205; Contract grant sponsor: Ministry of Education; Contract grant number: LH11033

quantum-chemical computations or are derived from the experiment. For example, the molecular property tensors (polarizabilites)[16] are derived from density functional theory computations on molecular fragments. The model not only provides a quantitatively correct prediction of the IRROA CID ratios, but also gives a deeper insight into the mechanism in question, revealing, for example, the role of the nonchiral substituents.

Method

The transition polarizability model

Let us have a system of N particles in an external beam of light described by the electric intensity $\mathbf{E}_e$, magnetic field $\mathbf{B}_e$, and electric field gradient $\nabla\mathbf{E}_e$. Because of the possibility to change the light frequency via the Raman scattering, each particle i ($i = 1 \ldots N$) is represented by an ensemble of induced electric dipoles $\boldsymbol{\mu}_{ia}$, magnetic dipoles $\mathbf{m}_{ia}$, and electric quadrupoles $\boldsymbol{\Theta}_{ia}$ each of them radiating at frequencies ω_a. For the electric dipole component, this situation is diagrammatically depicted in Figure 1. As frequency change is small in conventional Raman scattering ($(\omega_e - \omega_a)/\omega_e << 1$) and because of the expected continuity for $\omega_a \rightarrow \omega_e$, we can introduce the same phase approximation where the induced dipoles oscillate in phase with the impinging radiation. We assume that the dimension of the studied system is smaller than the wavelength of the light.

The multipoles induced by the electromagnetic field at each particle are as follows[16]

$$\boldsymbol{\mu}_{ia} = \boldsymbol{\alpha}_{ia}.\mathbf{E}_{ia} + \omega_a^{-1}\mathbf{G'}_{ia}.\mathbf{B}_{ia} + \frac{1}{3}\mathbf{A}_{ia}..\nabla\mathbf{E}_{ia} + \sum\nolimits_{a'}(\tilde{\boldsymbol{\alpha}}_{iaa'}.\mathbf{E}_{ia'} + \omega_{a'}^{-1}\tilde{\mathbf{G}}'_{iaa'}.\mathbf{B}_{ia'} + \frac{1}{3}\tilde{\mathbf{A}}_{iaa'}..\nabla\mathbf{E}_{ia'}), \quad (1a)$$

$$\mathbf{m}_{ia} = -\omega_a^{-1}\mathbf{G'}_{ia}.\mathbf{B}_0^{\cdot} - \sum\nolimits_{a'}\omega_{a'}^{-1}\tilde{\mathbf{G}}'_{iaa'}.\mathbf{B}_{ia'}^{\cdot}, \text{ and} \quad (1b)$$

$$\Theta_{ia} = \mathbf{A}_{ia}.\nabla\mathbf{E}_a + \sum\nolimits_{a'}\tilde{\mathbf{A}}_{iaa'}.\nabla\mathbf{E}_{a'}, \quad (1c)$$

where $\boldsymbol{\alpha}_{ia}$, $\mathbf{G'}_{ia}$, and $\mathbf{A}_{ia}$ are the respective electric dipole-electric dipole, electric dipole-magnetic dipole, and electric dipole-electric quadrupole polarizability. The tensors with tilde ($\tilde{\boldsymbol{\alpha}}_{iaa'}$, etc.) are analogous transitional polarizabilities.[16] The fields of frequency ω_a at each particle i are composed of the external field and contributions from other particles,

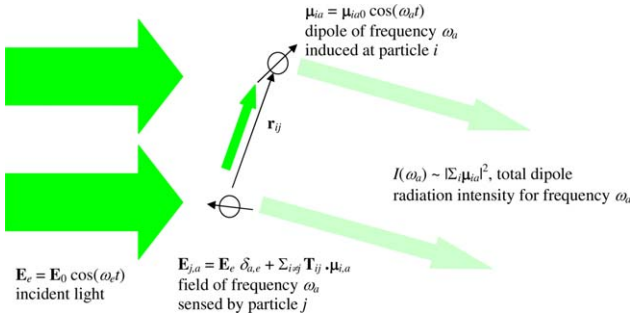

Figure 1. Interaction of particles with incident laser light described by the electric field intensity $\mathbf{E}_e$. [Color figure can be viewed in the online issue, which is available at wileyonlinelibrary.com]

$$\mathbf{E}_{ia} = \mathbf{E}_e\delta_{a,e} + \sum\nolimits_{j\neq i}(\mathbf{T}_{ij}\cdot\mu_{ja} - \nabla_i\mathbf{T}_{ij}\cdot\cdot\Theta_{ja}) + \ldots, \quad (2a)$$

$$\mathbf{B}_{ia} = \mathbf{B}_e\delta_{a,e} + c^{-1}\sum\nolimits_{j\neq i}\mathbf{T}_{ij}\cdot\mathbf{m}_{ja} + \ldots, \text{ and} \quad (2b)$$

$$\nabla\mathbf{E}_{ia} = \nabla\mathbf{E}_e\delta_{a,e} + \sum\nolimits_{j\neq i}(\nabla_i\mathbf{T}_{ij}\cdot\mu_{ja} - \sum\nolimits_{j\neq i}\nabla_i\nabla_i\mathbf{T}_{ij}\cdot\cdot\Theta_{ja}) + \ldots. \quad (2c)$$

Using the matrix perturbation theory (MPT) notation,[14,15] we can summarize eqs. (1a–c) and (2a–c) to compact forms,

$$\mathbf{M} = (\mathbf{P} + \tilde{\mathbf{P}}).\mathbf{F} = \Pi.\mathbf{F}, \quad (3)$$

and

$$\mathbf{F} = \mathbf{F}_e + \mathbf{X}.\mathbf{M}, \quad (4)$$

where

$$\mathbf{M} = \begin{pmatrix} \mathbf{M}_{1a_1} \\ \mathbf{M}_{1a_2} \\ \ldots \\ \mathbf{M}_{Na_M} \end{pmatrix}, \quad \mathbf{P} = \begin{pmatrix} \mathbf{P}_{1a_1} & 0 & .. & 0 \\ 0 & \mathbf{P}_{1a_2} & .. & 0 \\ .. & .. & .. & .. \\ 0 & 0 & .. & \mathbf{P}_{Na_M} \end{pmatrix},$$

$$\tilde{\mathbf{P}} = \begin{pmatrix} \tilde{\mathbf{P}}_{1a_1a_1} & \tilde{\mathbf{P}}_{1a_1a_2} & .. & 0 \\ \tilde{\mathbf{P}}_{1a_2a_1} & \tilde{\mathbf{P}}_{1a_2a_2} & .. & 0 \\ .. & .. & .. & .. \\ 0 & 0 & .. & \tilde{\mathbf{P}}_{Na_Ma_M} \end{pmatrix} \text{ and } \mathbf{F}_a = \begin{pmatrix} \mathbf{F}_{1a} \\ \mathbf{F}_{2a} \\ \ldots \\ \mathbf{F}_{Na} \end{pmatrix}.$$

Next, the frequency indices will be skipped. The particle/chromophore generalized moments, polarizabilities, and fields are

$$\mathbf{M}_i = \begin{pmatrix} \mu_i \\ \omega^{-1}\dot{\mu}_i \\ \mathbf{m}_i \\ \omega^{-1}\dot{\mathbf{m}}_i \\ \Theta_i/3 \\ \omega^{-1}\dot{\Theta}_i/3 \end{pmatrix},$$

$$\mathbf{P}_i = \begin{pmatrix} \boldsymbol{\alpha}_i & \mathbf{0} & \mathbf{0} & \mathbf{G}_i' & \mathbf{A}_i/3 & \mathbf{0} \\ \mathbf{0} & \boldsymbol{\alpha}_i & -\mathbf{G}_i' & \mathbf{0} & \mathbf{0} & \mathbf{A}_i/3 \\ \mathbf{0} & -\mathbf{G}_i'^t & \mathbf{0} & \mathbf{0} & \mathbf{0} & \mathbf{0} \\ \mathbf{G}_i'^t & \mathbf{0} & \mathbf{0} & \mathbf{0} & \mathbf{0} & \mathbf{0} \\ \mathbf{A}_i^t/3 & \mathbf{0} & \mathbf{0} & \mathbf{0} & \mathbf{0} & \mathbf{0} \\ \mathbf{0} & \mathbf{A}_i^t/3 & \mathbf{0} & \mathbf{0} & \mathbf{0} & \mathbf{0} \end{pmatrix},$$

and

$$\mathbf{F}_i = \begin{pmatrix} \mathbf{E}_i \\ \omega^{-1}\dot{\mathbf{E}}_i \\ \mathbf{B}_i \\ \omega^{-1}\dot{\mathbf{B}}_i \\ \nabla\mathbf{E}_i \\ \omega^{-1}\nabla\dot{\mathbf{E}}_i \end{pmatrix},$$

X is the distance matrix,

$$\mathbf{X}=\begin{pmatrix} 0 & \mathbf{X}_{12} & .. & \mathbf{X}_{1N} \\ \mathbf{X}_{21} & 0 & .. & \mathbf{X}_{2N} \\ .. & .. & .. & .. \\ \mathbf{X}_{N1} & \mathbf{X}_{N2} & .. & 0 \end{pmatrix},$$

$$\mathbf{X}_{ij}=\begin{pmatrix} \mathbf{T}_{ij} & 0 & 0 & 0 & -\nabla_i\mathbf{T}_{ij} & 0 \\ 0 & \mathbf{T}_{ij} & 0 & 0 & 0 & -\nabla_i\mathbf{T}_{ij} \\ 0 & 0 & \mathbf{T}_{ij}/c & 0 & 0 & 0 \\ 0 & 0 & 0 & \mathbf{T}_{ij}/c & 0 & 0 \\ \nabla_i\mathbf{T}_{ij} & 0 & 0 & 0 & -\nabla_i\nabla_i\mathbf{T}_{ij} & 0 \\ 0 & \nabla_i\mathbf{T}_{ij} & 0 & 0 & 0 & -\nabla_i\nabla_i\mathbf{T}_{ij} \end{pmatrix},$$

$\mathbf{T}_{ij,\alpha\beta}=\frac{1}{4\pi\varepsilon_0}\frac{3r_{ij,\alpha}r_{ij,\beta}-\delta_{\alpha\beta}r_{ij}^2}{r_{ij}^5}$ (in SI units), $\mathbf{r}_{ij}=\mathbf{r}_i-\mathbf{r}_j$, $\nabla_i=\frac{\partial}{\partial r_i}$, and ε_0 is vacuum permittivity, and $\mathbf{F}_e=\mathbf{E}_0$ for ω_e.

Defining **E** as the unitary matrix from (3) and (4), we get

$$\mathbf{F}=[\mathbf{E}-\mathbf{X}.\Pi]^{-1}\mathbf{F}_e, \tag{5}$$

and

$$\mathbf{M}=\Pi.[\mathbf{E}-\mathbf{X}.\Pi]^{-1}.\mathbf{F}_e=\tilde{\mathbf{P}}_t.\mathbf{F}_e. \tag{6}$$

Unlike for SERS,[14] we suppose that the contribution of Raman scattering to the laser radiation is small, that is, $\mathbf{E} >> \mathbf{X}.\Pi$. Then, the matrix inversion in eq. (6) can be replaced by a Taylor expansion, $\mathbf{M}=\Pi.[\mathbf{E}-\mathbf{X}.\Pi]^{-1}.\mathbf{F}_e=\tilde{\mathbf{P}}_t.\mathbf{F}_e$.

The transition polarizabilities are dependent on molecular transitions characterized by transitional frequencies ω_j, $\tilde{\mathbf{P}}_{i,a_1a_2}=\sum_j\tilde{\mathbf{P}}_{i,j}\delta(\omega_{a_1}-\omega_{a_2}-\omega_j)$. The matrix multiplication between variables *P* and *Q* with respect to the frequency indices needed in eq. (6) is realized as $(PQ)_{a_1a_2}\cong\int P_{a_1a'}Q_{a'a_2}d\omega_{a'}=\sum_{i,j}P_iQ_j\delta(\omega_{a_1}-\omega_{a_2}-\omega_i-\omega_j)$.

The multipoles of the whole system written in the common origin gauge are defined as

$$\mu_\alpha=\sum_{i=1..N}M_{i\alpha}, \tag{7a}$$

$$m_\alpha=\sum_{i=1..N}(M_{i\alpha+6}+\omega\epsilon_{\alpha\beta\gamma}r_{i\beta}M_{i,\gamma+3}/2), \tag{7b}$$

and

$$\Theta_{\alpha\beta}=\sum_{i=1..N}(3M_{i,(\alpha\beta)+12}+(3/2)(M_{i,\alpha}r_{i\beta}+M_{i,\beta}r_{i\alpha})-\delta_{\alpha\beta}r_{i\gamma}M_{i,\gamma}). \tag{7c}$$

Because of the symmetry of the quadrupole, $\Theta_{\alpha\beta}=\Theta_{\beta\alpha}$, we can introduce a common index $(\alpha\beta)=1\ldots6$ for the independent components, and the dimension of $\tilde{\mathbf{P}}_t$ will be 24 times the number of particles, for all frequencies ω_k, $k=1\ldots N_t$, generated by the interactions.

From (7a and b) and (1a–c), we get the total transition polarizabilities as

$$\tilde{\alpha}_{ae,\alpha\beta}=\frac{\partial\mu_{a,\alpha}}{\partial E_{e\beta}}=\sum_{i=1}^{N}\tilde{P}_{t,ae,i,\alpha,\beta}, \tag{8a}$$

$$\tilde{G'}_{ae,\beta\alpha}=-\frac{\partial m_{a,\alpha}}{\omega^{-1}\partial E_{e\beta}}=-\sum_{i=1}^{N}\left(\tilde{P}_{t,ae,i,\alpha+6,\beta+3}+\frac{\omega}{2}\epsilon_{\alpha\beta\gamma}r_{i\beta}\tilde{P}_{t,ae,i,\gamma+3,\beta+3}\right), \tag{8b}$$

$$\tilde{A}_{ae,\gamma,\alpha\beta}=\frac{\partial\Theta_{a,\alpha\beta}}{\partial E_{e\gamma}}=\sum_{i=1}^{N}\left(3\tilde{P}_{t,ae,i,(\alpha\beta)+12,\gamma}+\frac{3}{2}\left(\tilde{P}_{t,ae,i,\alpha,\gamma}r_{i\beta}+\tilde{P}_{t,ae,i,\beta,\gamma}r_{i\alpha}\right)-\delta_{\alpha\beta}r_{i\epsilon}\tilde{P}_{t,ae,i,\epsilon,\gamma}\right). \tag{8c}$$

The backscattered (180°) circular-polarized ROA and Raman intensities are[7,17]

$$I_{\mathrm{ROA}}(\omega_a)=16Kc^{-1}(9\alpha_{ae,\alpha\beta}G'_{ae,\alpha\beta}-3\alpha_{ae,\alpha\alpha}G'_{ae,\beta\beta}+\omega\alpha_{ae,\alpha\beta}\epsilon_{\alpha\gamma\delta}A_{ae,\gamma,\delta\beta}), \tag{9a}$$

$$I_{\mathrm{Raman}}(\omega_a)=6K(\alpha_{ae,\alpha\alpha}\alpha_{ae,\beta\beta}+7\alpha_{ae,\alpha\beta}\alpha_{ae,\alpha\beta}), \tag{9b}$$

where *K* is a constant, *c* is the speed of light, and $\varepsilon_{\alpha\beta\gamma\gamma}$ is the antisymmetric tensor; the Einstein summation convention is used. A part corresponding to antisymmetric resonance Raman scattering possible for certain metal ions[7] was ignored in eq. (9a and 9b). Formulas that are more general can be found in Refs. [7] and [16]. For the Eu(fod)$_3$ complex, a very low degree of circularity ($<<1$) measured with our ROA instrument indicates a symmetric scattering only. Stokes spectra were obtained by multiplication by a temperature-correction factor[17] and convolution with Lorentzian curves,

$$S(\omega)=\sum_a I_a\left[1-\exp\left(-\frac{\omega_a}{kT}\right)\right]^{-1}\frac{1}{\omega_a}\left[4\left(\frac{\omega-\omega_a}{\Delta}\right)^2+1\right]^{-1}, \tag{10}$$

where *k* is the Boltzmann constant, *T* is the temperature (298 K), and Δ = 15 cm^{-1}.

Quantum mechanical computations

For test molecules involving camphor and Eu(fod)$_3$ complex parts (Fig. 2), the geometry was optimized by energy minimization within the Gaussian[18] program environment. For camphor, the B3PW91[19,20]/6-311++G** computational levels were used with the conductor-like polarizable continuum model (CPCM)[21,22] solvent environment for carbontetrachloride to simulate nonpolar solvents used in IRROA experiments.[9] The optimized geometry was used for computation of the ROA polarizability derivatives which were then converted to the transitional polarizabilities ($\tilde{\alpha}$, $\tilde{\mathbf{G}}'$, and $\tilde{\mathbf{A}}$) as, for example, $\tilde{\boldsymbol{\alpha}}_{aa'}=\sum_i\frac{\partial\boldsymbol{\alpha}}{\partial Q_i}\langle1|Q|0\rangle\delta(\omega_i-\omega_a+\omega_{a'})$, where Q_i is the coordinate of the vibrational normal mode *i*.

Four initial Eu(fod)$_3$ geometries with extended fod conformers were tested, based on prevalent conformations of similar species in crystals.[23–26] Crystal structure of pure Eu(fod)$_3$ is not known to us. The first geometry possessed C_3 symmetry

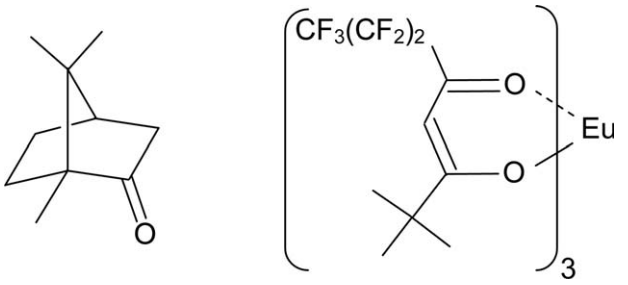

Figure 2. (1R)-(+)-camphor (1,7,7-trimethylbicyclo [2.2.1]heptan-2-one, left), and the $Eu(fod)_3$ complex [(Eu^{III}-tris(1,1,1,2,2,3,3-heptafluoro-7,7-dimethyl-4,6-octanedionate), right]. [Color figure can be viewed in the online issue, which is available at wileyonlinelibrary.com]

with the *t*-butyl residues pointing to the same direction, whereas another exhibited the C_s symmetry with one of the residues pointing in the opposite direction. The two remaining conformers, both of the C_1 symmetry, were created by a slight ligand twist from the C_3 and C_s species. Complete minimizations were performed, without any symmetry or coordinate constraints. The C_3 symmetry of the first conformer did not change during the energy minimization and this geometry also provided the lowest energy at the BPW91/6-31G** level. It was thus chosen as the most plausible form in the complex with camphor. The MWB52[27] basis set and effective core potential were used for Eu. Although such conformer construction provides a basic information about the behavior of the Eu(fod) system and is consistent with available x-ray data, one should note that a full conformer search goes beyond the scope of this study, primarily focused at the origin of the IRROA signal.

The enantiomers of the $Eu(fod)_3$ C_3 optimized structure were created ("L" and "R," a left and right propeller) and attached to (1R)-(+)-camphor so that the camphor pointed in the opposite direction, relative to the *t*-butyls. The geometries of such complexes were optimized at the PM7[28] level by the Mopac program[29] using the Sparkle[30] representation of the Eu^{3+} ion, and Hartree-Fock (HF)/6-31G/MWB52, BPW91/6-31G**/MWB52, B3LYP/6-31G**/MWB52, and B3LYP/6-31++G**/MWB52 levels by Gaussian. The dispersion correction[31] was additionally applied, indicated by a letter "D" appended to the method abbreviation (BPW91-D, etc.). In some computations, the solvent was simulated by the CPCM model.

For the BPW91/6-31G**/MWB52-optimized geometries of the $Eu(fod)_3$-camphor complexes, the polarizabilities needed to simulate the ROA spectrum were calculated separately for the camphor and three fod^- residues at the B3PW91/6-311++G**/CPCM level. For camphor, this procedure provided almost the same Raman and ROA spectra as the full optimization, which we consider sufficient for the purpose of the modeling. For the Eu^{3+} ion, the transition electric dipole polarizability (α) was estimated from the experimental spectrum of the $Eu(fod)_3$ complex; tensors **G′** and **A** were set to zero in the local origin.

Results and Discussion

Model tests

To illustrate the implementation and performance of the transition polarizability model (TPM), the Raman and ROA spectra of camphor are compared in Figure 3, top, as generated by the IRROA model presented above, and by a direct computation from the polarizability derivatives. As it is apparent, the Raman and ROA intensities are indistinguishable.

As a more advanced test, we simulated SERS and SEROA spectra of the 1R-(+)-camphor in the vicinity of a polarizable

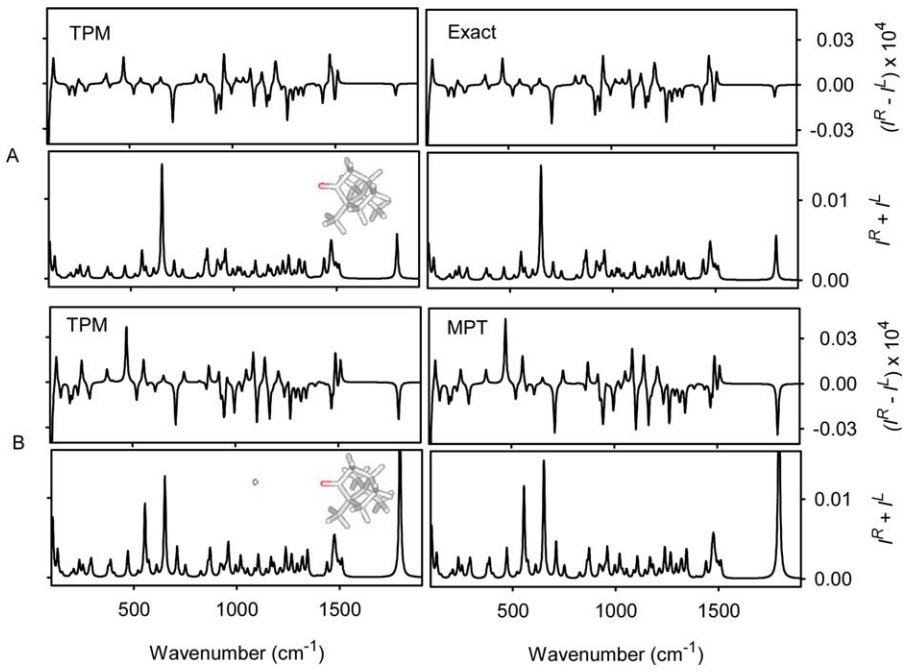

Figure 3. (A) Comparison of the TPM computation with the exact *ab initio* result for an isolated (1R)-(+)-camphor molecule, and (B) TPM and MPT simulations of the SEROA and SERS spectra of (1R)-(+)-camphor in the vicinity of a polarizable sphere. [Color figure can be viewed in the online issue, which is available at wileyonlinelibrary.com]

sphere. The sphere of an isotropic polarizability $\alpha = 2500$ was positioned on the C═O bond axis, 10 Å from the oxygen atom. In Figure 3, bottom, we compare the TPM model with the full MPT[14] formalism.

The two models provide very similar spectra with only minor (~10–20%) differences in the spectral intensities. The difference is due to the TPM approximation based on a single origin, as used for the tensors of the camphor molecule. For the MPT computation, individual atomic positions for the polarizability tensor atomic derivatives are considered. As expected for the relatively large 10 Å distance, such difference has little influence on the spectral pattern. The vicinity of the sphere leads to an overall enhancement of spectral intensities, small changes in relative Raman band intensities, and larger changes of relative ROA band intensities. Occasionally, some ROA bands even switch signs (e.g., at 746 and 1464 cm^{-1}).

Eu-camphor (monoligand) complex

In this model, one europium atom modeled as a polarizable sphere was placed on the C═O camphor axis, 2.3 Å from the oxygen atom. This Eu … O distance approximately corresponds to the distances found in similar complexes experimentally.[26,32] Relative Eu transition polarizabilities were estimated by a band fit of the experimental Raman $Eu(fod)_3$ spectrum,[9] and are listed in Table 1.

The simulated IRROA and Raman spectra are plotted in Figure 4. Apparently, the chiral camphor can induce a single-sign ROA signal copying the Raman intensities. The sign of ROA, however, depends on the molecular chirality. The result is in a qualitative agreement with the IRROA experiment,[9] where the Raman $Eu(fod)_3$ spectrum remains virtually unchanged on the complexation, the ROA signal is of a predominant sign, and the intensity approximately follows the relative Raman strengths. However, the calculated CID $\sim 10^{-6}$ ROA/Raman ratio is much smaller than for the conventional ROA (where CID $\sim 10^{-4}$, compare the *y*-scales in Figs. 3 and 4). The single-ligand model is thus unable to reproduce the IRROA observations where much larger CIDs were found in a quantitative way.

On the other hand, the all-ligand model with the L- and R-$Eu(fod)_3$·(1R)-(+)-camphor complexes presented in Figure 5

Table 1. Transition Eu^{3+} polarizabilities used in spectral modeling.

Transition	ω_i (cm^{-1})	α_i
0	0	20
1	1442	6
2	1462	6
3	1532	29
4	1634	4.3
5	1726	9
6	1801	18
7	1871	18
8	1936	15
9	2006	14
10	2065	10
11	2124	4.32
12	2439	16.3

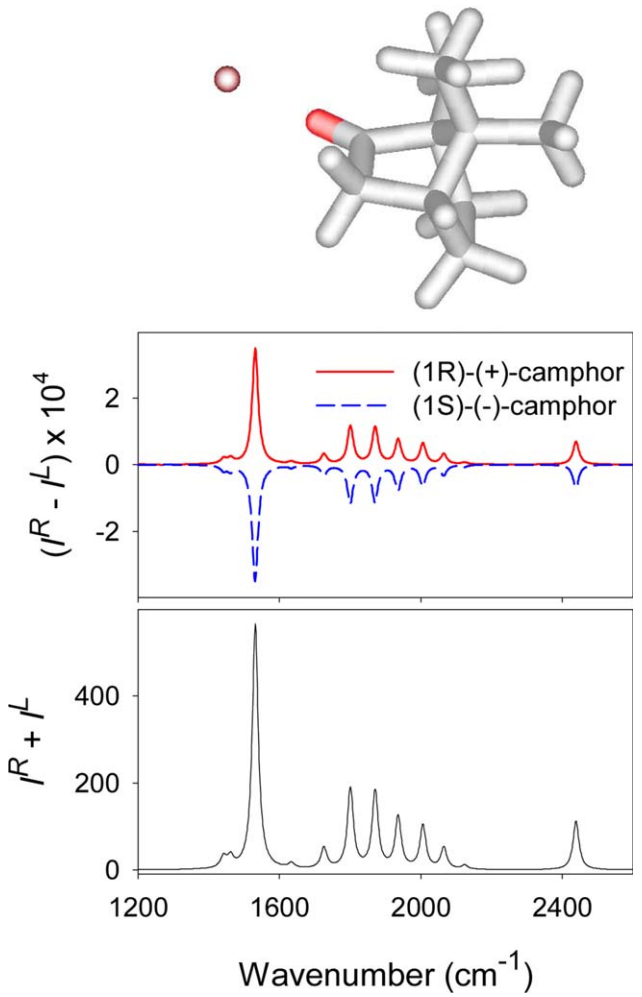

Figure 4. Simulated IRROA and Raman spectra of the complexes of (R)-(geometry displayed) and (S)-camphor with one Eu atom.

does reproduce also the experimental CID IRROA magnitudes of $\sim 10^2$–10^3, including finer changes in the Raman spectral profile. The fod^- residues and their chiral arrangement thus appear necessary to induce measurable chirality within the europium ion.

The plus ROA sign simulated for the L-$Eu(fod)_3$·(1R)-(+)-camphor complex (Fig. 5) is consistent with the experiment (Fig. 6, reported in detail in Ref. [9]). The simulation, however, strongly underestimates the relative ROA intensity for the intense Raman band at 1532 cm^{-1}, and predicts an opposite sign of the weaker signal at 2439 cm^{-1}. These finer differences between the theoretical and experimental ROA spectra are attributed to a specific Eu–ligand interaction that could not be included in the electrodynamic model.

The calculated relative energies of the L- and R-$Eu(fod)_3$·(1R)-(+)-camphor complexes are listed in Table 2. The differences are smaller than 1 kcal/mol, which is on the brim of the computational error. For the HF method, the addition of the dispersion correction switches the order and stabilizes the R-conformer, whereas for the BPW91 computation it makes the L conformer favored already without the dispersion more stable. The addition of the CPCM solvent to the computations

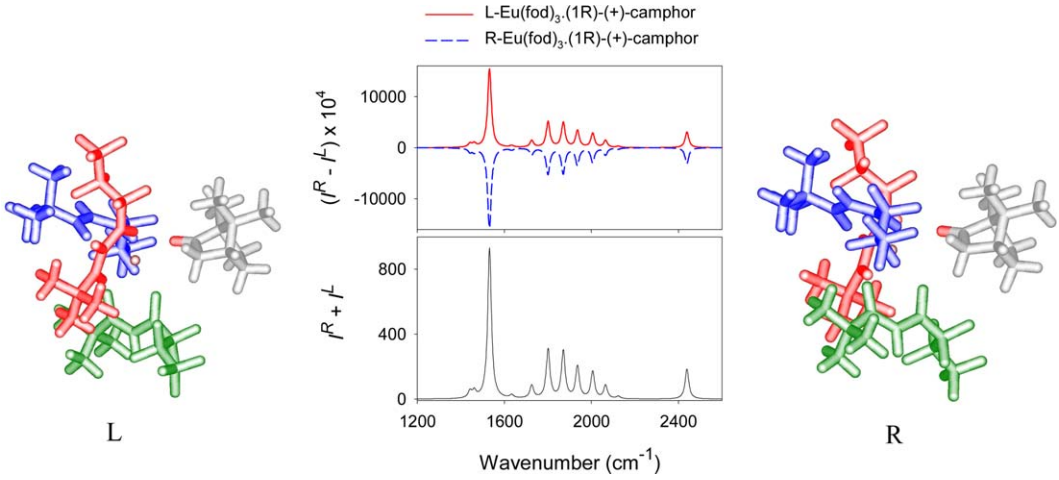

Figure 5. Simulated IRROA and Raman spectra of the complexes of (1R)-(+)-camphor and L and R—Eu(fod)$_3$ conformers. The geometries optimized at the BPW91/6-31G**/MWB52 level are displayed.

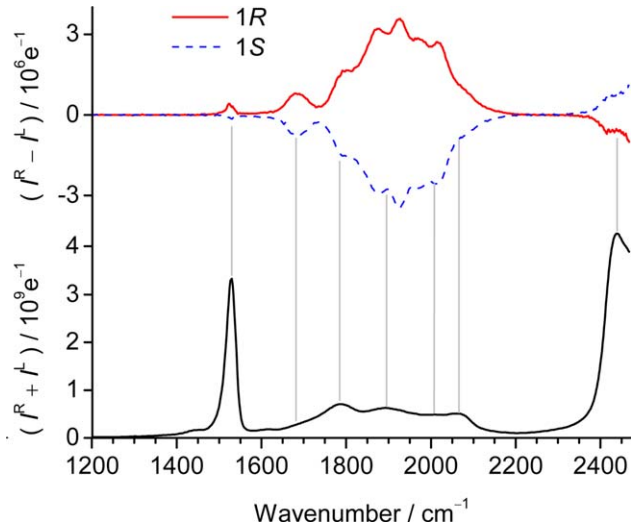

Figure 6. Experimental IRROA and Raman spectra of a complex of (1*R*)- or (1*S*)-camphor (10 mM) and the Eu(fod-d$_9$)$_3$ (1.0 mM) in *n*-hexane. For experimental details, see Ref. [9]. [Color figure can be viewed in the online issue, which is available at wileyonlinelibrary.com]

with the 6-31G** basis set favors the R conformer, and this is yet again reversed when the larger 6-31++G** basis set is used. The positive experimental ROA sign for (1R)-(+)-camphor (Fig. 6) suggests the dominance of the L-Eu(fod)$_3$·(1R)-(+)-camphor complex (cf. Fig. 5), in agreement with the presumably most advanced B3LYP-D/6-31++G**/MWB52/CPCM method predicting a stabilization energy of 0.35 kcal/mol for this conformer. However, this agreement may well be only accidental. Indeed, the full conformational search and determination of the association constant is an extremely complex task.[33–38]

Table 2. Relative energies (kcal/mol) of the L- and R-Eu(fod)$_3$.(1R)-(+)-camphor complexes calculated at different approximation levels.

Method	*L*	*R*
PM7	0.36	0.00
HF/6-31G/MWB52	−0.97	0.00
HF-D/6-31G/MWB52	0.33	0.00
BPW91/6-31G**/MWB52	−0.01	0.00
BPW91-D/6-31G**/MWB52	−0.12	0.00
BPW91-D/6-31G**/MWB52/CPCM	0.04	0.00
B3LYP-D/6-31G**/MWB52/CPCM	1.03	0.00
B3LYP-D/6-31++G**/MWB52/CPCM	−0.35	0.00

Conclusions

Based on the semiclassical concept of the transitional polarizabilities, we formulated an approximate theory of the IRROA. It was combined with quantum mechanical computations on molecular fragments and experimentally-derived polarizabilities of the europium ion. The theory was successfully tested to reproduce SERS/SEROA spectra against the MPT. For the model Eu(fod)$_3$·(1R)-(+)-camphor complex, it provided an approximate (both qualitative and quantitative) agreement with experimental IRROA data, including an indication of AC. The modeling clearly reveals the prevailing mechanism of the IRROA induction, contributes to our understanding of the phenomenon, and suggests directions of future experimental and theoretical efforts. In particular, the role of the achiral parts and complex geometries and energetics needs to be better established if AC is to be reliably determinate by IRROA in the future.

Keywords: induced resonance Raman optical activity · europium complexes · density functional computations · light scattering

How to cite this article: Yamamoto S, Bouř P. *J. Comput. Chem.* **2013**, *34*, 2152–2158. DOI: 10.1002/jcc.23370

[1] T. Eriksson, S. Björkman, B. Roth, Å. Fyge, P. Höuglund, *Chirality* **1995**, *7l*, 44.
[2] J. Drenth. Principles of Protein X-ray Crystallography; Springer-Verlag: Berlin, **1994**.
[3] M. Srebro, N. Govind, W. A. d. Jong, J. Autschbach, *J. Phys. Chem. A* **2011**, *115*, 10930.

[4] T. D. Crawford, M. C. Tam, M. L. Abrams, *J. Phys. Chem. A* **2007**, *111*, 12057.
[5] D. M. McCann, P. J. Stephens, *J. Org. Chem.* **2006**, *71*, 6074.
[6] S. D. Zhao, L. Shen, D. Q. Luo, H. J. Zhu, *Curr. Org. Chem.* **2011**, *15*, 1843.
[7] L. Nafie. Vibrational Optical Activity: Principles and Applications; Wiley: Chichester, **2011**.
[8] C. Merten, H. Li, X. Lu, A. Hartwiga, L. A. Nafie, *J. Raman Spectrosc.* **2010**, *41*, 1563.
[9] S. Yamamoto, P. Bouř, *Angew. Chem. Int. Ed.* **2012**, *51*, 11058.
[10] J. A. Koningstein, *Russ. Chem. Rev.* **1973**, *42*, 834.
[11] J. A. Koningstein, *J. Chem. Phys.* **1967**, *46*, 2811.
[12] J. Grunenberg. Computational Spectroscopy; Wiley: Weinheim, **2011**.
[13] B. G. Janesko, G. E. Scuseria, *J. Chem. Phys.* **2006**, *125*, 124704.
[14] V. Novák, J. Šebestík, P. Bouř, *J. Chem. Theory Comput.* **2012**, *8*, 1714.
[15] P. Bouř, *J. Chem. Phys.* **2007**, *127*, 136101.
[16] L. D. Barron. Molecular Light Scattering and Optical Activity; Cambridge University Press: Cambridge, **2004**.
[17] P. L. Polavarapu, *J. Phys. Chem.* **1990**, *94*, 8106.
[18] M. J. Frisch, G. W. Trucks, H. B. Schlegel, G. E. Scuseria, M. A. Robb, J. R. Cheeseman, G. Scalmani, V. Barone, B. Mennucci, G. A. Petersson, H. Nakatsuji, M. Caricato, X. Li, H. P. Hratchian, A. F. Izmaylov, J. Bloino, G. Zheng, J. L. Sonnenberg, M. Hada, M. Ehara, K. Toyota, R. Fukuda, J. Hasegawa, M. Ishida, T. Nakajima, Y. Honda, O. Kitao, H. Nakai, T. Vreven, J. Montgomery, J. A. , J. E. Peralta, F. Ogliaro, M. Bearpark, J. J. Heyd, E. Brothers, K. N. Kudin, V. N. Staroverov, R. Kobayashi, J. Normand, K. Raghavachari, A. Rendell, J. C. Burant, S. S. Iyengar, J. Tomasi, M. Cossi, N. Rega, J. M. Millam, M. Klene, J. E. Knox, J. B. Cross, V. Bakken, C. Adamo, J. Jaramillo, R. Gomperts, R. E. Stratmann, O. Yazyev, A. J. Austin, R. Cammi, C. Pomelli, J. W. Ochterski, R. L. Martin, K. Morokuma, V. G. Zakrzewski, G. A. Voth, P. Salvador, J. J. Dannenberg, S. Dapprich, A. D. Daniels, O. Farkas, J. B. Foresman, J. V. Ortiz, J. Cioslowski, D. J. Fox. Gaussian 09, Revision C01, Gaussian Inc.: Wallingford CT, **2009**.
[19] J. P. Perdew, K. Burke, Y. Wang, *Phys. Rev. B* **1996**, *54*, 16533.
[20] A. D. Becke, *J. Chem. Phys.* **1993**, *98*, 5648.
[21] A. Klamt, V. Jonas, T. Burger, J. C. W. Lohrentz, *J. Phys. Chem. A* **1998**, *102*, 5074.
[22] A. Klamt, G. Schuurmann, *J. Chem. Soc. Perkin Trans.* **1993**, *2*, 799.
[23] L. F. Lindoy, H.C. Lip, H. W. Louie, M. G. B. Drew, M. J. Hudson, *Chem. Commun.* **1977**, 778.
[24] V. A. Petrov, W. J. Marshall, V. V. Grushin, *Chem. Commun.* **2002**, *0*, 520.
[25] J. Yu, L. Zhou, H. Zhang, Y. Zheng, H. Li, R. Deng, Z. Peng, Z. Li, *Inorg. Chem.* **2005**, *44*, 1611.
[26] E. R. dos Santos, R. O. Freire, N. B. da Costa, F. A. A. J. Paz, C. A. de Simone, S. A. Júnior, A. A. S. Araújo, L. A. O. Nunes, M. E. de Mesquita, M. O. Rodrigues, *J. Phys. Chem. A* **2010**, *114*, 7928.
[27] M. Dolg. In Part 1: Fundamentals, Theoretical and Computational Chemistry; P. Schwerdtfeger, Ed.; Elsevier: Amsterdam, **2002**, p. 793.
[28] J. J. P. Steward, *J. Mol. Modeling* **2007**, *13*, 1173.
[29] J. J. P. Steward, MOPAC2012; Steward Computational Chemistry: Colorado Springs, **2012**.
[30] R. O. Freire, A. M. Simas, *Int. J. Quantum Chem.* **2011**, *111*, 1734.
[31] T. Schwabe, S. Grimme, *Phys. Chem. Chem. Phys.* **2007**, *9*, 3397.
[32] H. Tsukube, S. Shinoda, *Chem. Rev.* **2002**, *102*, 2389.
[33] M. K. Gilson, J. A. Given, B. L. Bush, J. A. McCammon, *Biophys. J.* **1997**, *72*, 1047.
[34] H. X. Zhou, M. K. Gilson, *Chem. Rev.* **2009**, *109*, 4092.
[35] S. Grimme, J. Antony, S. Ehrlich, H. Krieg, *J. Chem. Phys.* **2010**, *132*, 154104.
[36] M. P. Waller, H. Kruse, C. Mück-Lichtenfeld, S. Grimme, *Chem. Soc. Rev.* **2012**, *41*, 3119.
[37] V. Parchaňský, P. Matějka, B. Dolenský, M. Havlík, P. Bouř, *J. Mol. Struct.* **2009**, *934*, 117.
[38] J. Kessler, M. Jakubek, B. Dolenský, P. Bouř, *J. Comput. Chem.* **2012**, *33*, 2310.

Received: 15 April 2013
Revised 7 June 2013
Accepted: 17 June 2013
Published online on 4 July 2013